

# Dynamical generation of charmonium-like tetraquarks in an off-shell coupled-channel formalism

Hee-Jin Kim<sup>1</sup> and Hyun-Chul Kim<sup>2,1,3</sup>

<sup>1</sup>*Institute of Quantum Science, Inha University, Incheon 22212, Republic of Korea*

<sup>2</sup>*Department of Physics, Inha University, Incheon 22212, Republic of Korea*

<sup>3</sup>*School of Physics, Korea Institute for Advanced Study (KIAS), Seoul 02455, Republic of Korea*

(Dated: March 26, 2026)

We investigate the dynamical generation of charmonium-like ( $I = 0$ ) with spin-parity  $J^{PC} = 0^{++}, 1^{++}, 2^{++}$ , and  $3^{--}$  in the mass range of 3.6 to 4.3 GeV. We employ the off-shell coupled-channel formalism, constructing kernel amplitudes from effective Lagrangians that respect heavy-quark spin-flavor and chiral symmetries. To focus solely on dynamically generated states, we explicitly exclude  $s$ -channel pole diagrams and include only  $t$ - and  $u$ -channel meson exchanges. Solving the integral equations, we identify six poles in the complex energy plane. In the scalar ( $0^{++}$ ) sector, we find a bound state below the  $D\bar{D}$  threshold and a resonance at  $\sqrt{s_R} = (3861 - i23)$  MeV. For the axial-vector ( $1^{++}$ ) sector, the experimentally observed  $\chi_{c1}(3872)$  is reproduced as a bound state near the  $D\bar{D}^*$  threshold, alongside a broader resonance at  $(3961 - i32)$  MeV, which is a plausible candidate for the  $X(3940)$ . Furthermore, we find a narrow tensor ( $2^{++}$ ) state at 4005 MeV and a vector ( $3^{--}$ ) state at 4030 MeV. The present results demonstrate that coupled-channel dynamics, particularly involving the  $D^*\bar{D}^*$  channel, play a crucial role in the formation of these charmonium-like exotic states.

## I. INTRODUCTION

The discovery of the  $\chi_{c1}(3872)$  (also known as  $X(3872)$ ) by the Belle Collaboration [1] opened a new era in the study of the heavy hadrons. Its extremely narrow width, isospin-violating decays, and proximity to the  $D^0\bar{D}^{*0}$  threshold were not able to accommodate a simple interpretation within conventional quark models (CQM). Since then, a large number of charmonium-like structures, often referred to as the  $XYZ$  states, have been reported by the Belle, BaBar, BESIII, and LHCb Collaborations in various hadronic processes such as  $B$  decays, initial-state radiation, two-photon fusion, and  $e^+e^-$  annihilation (see the reviews [2–7]). While a few of the observed structures can still be understood as ordinary charmonia [8–10], e.g.,  $\psi_2(3823)$  and  $\psi_3(3842)$  as the  $1D$  spin-triplet [11] or  $\chi_{c2}(3930)$  as the  $2^3P_2$   $c\bar{c}$  state [12, 13], many others lie close to open-charm thresholds and show behaviors that are difficult to describe with a naive  $c\bar{c}$  interpretation. Several of these states have unexpectedly narrow widths, decay modes or branching ratios that do not follow quark-model predictions.

Their properties often depend sensitively on nearby threshold, for instance  $D^{(*)}\bar{D}^{(*)}$  channels, indicating that coupled-channel dynamics play a crucial role. As a result, the spectrum in the charmonium sector (especially in the  $\sqrt{s} \approx 3.7$  to 4.1 GeV region) cannot be viewed as typical radial or orbital excitations of  $c\bar{c}$  states. Instead, it has become a mixture of various structures affected by threshold effects and channel mixing [3, 4]. In such a regime, the investigation of coupled-channel dynamics provides essential information: They are directly influenced by how each state couples to nearby open-flavor channels, such as through threshold effects or triangle singularities, and therefore offer a practical guide to the underlying configurations of these hidden-charm candidates. The theoretical interpretation of the charmonium-like spectrum remains highly nontrivial, and many models have been developed to describe the observed structures. Beyond the CQM description, compact tetraquarks [14–20] and hadronic molecules generated by near-threshold dynamics [3–7] constitute two of the most widely discussed pictures. Additional mechanisms such as hybrid charmonia, hadroquarkonium configurations, and kinematic effects (cusp-like structures or triangle singularities) have also been considered in describing specific candidates.

A particularly important aspect of this sector is that various channels are open near  $D\bar{D}$ ,  $D\bar{D}^*$ ,  $D^*\bar{D}$ , and  $D^*\bar{D}^*$  thresholds, a feature that requires the consideration of coupled-channel dynamics. While the Bethe-Salpeter (BS) equation provides a proper theoretical framework for treating multi-channel hadronic scattering, it is practically too complicated to deal with the four-dimensional BS equation. To overcome the complexities of solving the full BS equation, various approximations have been developed such as the on-shell approximation and three-dimensional reductions. In the current work, we will take a three-dimensional reduction known as the Blankenbecler-Sugar (BbS) scheme, which offers a significant advantage by preserving both the unitarity and the off-shell contributions of the coupled-channel BbS integral equations. The kernel amplitudes for the BbS equation are constructed by computing the Feynman invariant amplitudes based on effective Lagrangians. Since we are mainly interested in how the tetraquark states are dynamically generated, we only include the  $t$ - and  $u$ -channel amplitudes. To preserve the unitarity and to consider the structure of hadrons, it is essential to introduce form factors at each vertex, which causes uncertainties in numerical results. To minimize them, we introduce the reduced cutoff mass defined by the

subtraction of the corresponding cutoff mass and exchange hadron mass, which will be discussed in more detail later. Having solved the three-dimensional coupled BbS equations, we can derive the transition amplitudes containing the coupled-channel effects. Surveying pole positions of the transition amplitudes in the complex energy plane, we can determine the masses and widths of the tetraquark states corresponding to the poles. This coupled-channel formalism has been successfully applied to describing various hadronic reactions. In Refs. [21–23], it was shown how the axial-vector mesons such as  $a_1(1260)$ ,  $b_1(1235)$ , and  $h_1(1415)$  are dynamically generated from pseudoscalar-vector meson scattering. The production mechanisms of the hidden-charm pentaquarks with strangeness varying from 0 to  $-3$  were also investigated within the same coupled-channel formalism [24–26], and the  $P_{c\bar{c}}$ 's were interpreted as the molecular states associated with the heavy mesons  $\bar{D}(\bar{D}^*)$  and singly heavy baryons  $\Sigma_c(\Sigma_c^*)$ . The same theoretical framework was also employed to describe the  $D_{s0}^*(2317)$  as a  $DK$  molecular state [27] and to investigate the doubly-charmed tetraquark state  $T_{cc}$  [28]. A merit of this off-shell coupled-channel formalism can be found in the fact that it incorporates relevant symmetries and energy scales across not only  $S$  waves but also higher partial-wave components.

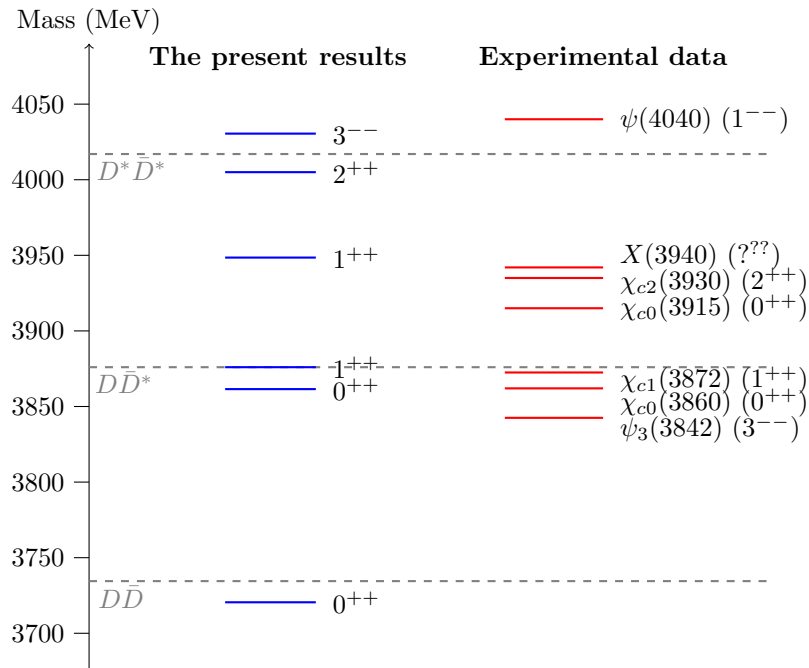


FIG. 1. Mass spectrum of hidden-charm states in the range of 3.7–4.1 GeV. The lines in the left column indicate the resonance states obtained in the present work, whereas those in the right column denote the experimental data for the states with  $c\bar{c}$  content [29].

In the present study, we investigate the dynamical generation of charmonium-like states ( $\chi_{cJ}$  and  $\psi_J$  states) with the hidden-charm  $c\bar{c}$  content in the range of center-of-mass energies from 3.7 to 4.1 GeV. Figure 1 summarizes the results of this work in comparison with the conventional  $c\bar{c}$  states listed by the Particle Data Group (PDG) [29]. Since we mainly focus on the dynamical generation of exotic states, we intentionally exclude  $s$ -channel pole diagrams from the kernel amplitudes to ensure that all resonances are dynamically generated solely from coupled-channel dynamics. Consequently, we identify six  $c\bar{c}$  states by solving the coupled-channel integral equations. Three of these states are consistent with the experimentally observed charmonium-like structures, such as the  $\chi_{c1}(3872)$  near the  $D\bar{D}^*$  threshold. Furthermore, our results predict three additional  $c\bar{c}$  resonances that are dynamically generated through coupled-channel dynamics.

This paper is organized as follows. In Section II, we explain the general formalism for the coupled-channel BbS scheme in detail. The interactions between heavy mesons, charmonia, and light mesons are derived from effective Lagrangians governed by heavy-quark spin-flavor and chiral symmetries, which serve as the basis for constructing the kernel matrices. In Section III, we discuss the numerical results for each spin-parity assignment. By scanning the transition amplitudes, we extract pole positions and coupling strengths to various hadronic channels to elucidate their dynamical origins and properties. We will also discuss the physical origin of the agreement and discrepancy with the experimental data in detail. Section IV is devoted to a summary of our numerical analysis and concluding remarks.

## II. GENERAL FORMALISM

The scattering amplitude of the  $i \rightarrow f$  process is given by

$$S_{fi} = \delta_{fi} - (2\pi)^4 \delta^{(4)}(P_f - P_i) \mathcal{T}_{fi}, \quad (1)$$

where  $P_i$  and  $P_f$  are the total four-momenta of the initial and final states, respectively. The transition amplitudes  $\mathcal{T}_{fi}$  contain nontrivial information on how the resonances and bound states are generated dynamically. The  $\mathcal{T}_{fi}$  are obtained by solving the Bethe-Salpeter (BS) equation with the two-body Feynman kernel amplitudes:

$$\mathcal{T}_{fi}(p, p'; s) = \mathcal{V}_{fi}(p, p'; s) \frac{1}{(2\pi)^4} \sum_k \int d^4 q_k \mathcal{V}_{fk}(p, q_k; s) G_k(q_k; s) \mathcal{T}_{ki}(q_k, p'; s), \quad (2)$$

where  $p$  and  $p'$  denote respectively the relative four-momenta of the initial and final states, and  $q_k$  is the off-shell four-momentum for intermediate states in the center-of-mass (CM) frame. The variable  $s \equiv P_i^2 = P_f^2$  is the square of the total energy. The indices  $i$ ,  $f$ , and  $k$  indicate the initial, final, and intermediate states, respectively. The index  $k$  runs over all relevant intermediate channels to nonstrange hidden-charm states. The schematic diagram for the coupled BS equation (2) is depicted in Fig. 2.

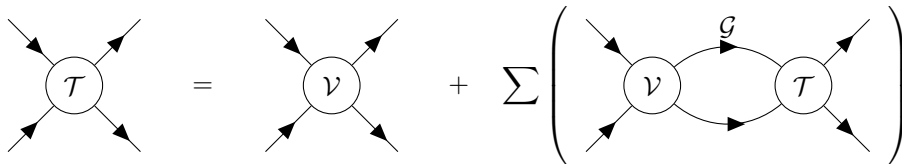


FIG. 2. Schematic diagram for the two-body coupled integral equations.

Since it is computationally demanding to solve the four-dimensional BS integral equations, we introduce a three-dimensional reduction approach. While there are various ways for this reduction, we adopt the Blankenbecler-Sugar formalism (BbS) [30, 31], where the two-body propagator is taken to be

$$G_k(q_k) = \frac{\pi}{\omega_1^k \omega_2^k} \delta \left( q_k^0 - \frac{\omega_1^k - \omega_2^k}{2} \right) \frac{\omega_1^k + \omega_2^k}{s - (\omega_1^k + \omega_2^k)^2 + i\epsilon}, \quad (3)$$

where  $\omega_{1(2)}^k = \sqrt{\mathbf{q}_k^2 + (m_{1(2)}^k)^2}$  is the energy of the particle 1(2) in the channel  $k$  on the mass shell. We then insert  $G_k$  in Eq. (2), so that we obtain the three-dimensional coupled integral equation for each  $q_k^0$ :

$$T_{fi}(\mathbf{p}, \mathbf{p}'; s) = V_{fi}(\mathbf{p}, \mathbf{p}'; s) + \frac{1}{(2\pi)^3} \sum_k \int \frac{d^3 q_k}{2\omega_1^k \omega_2^k} \frac{\omega_1^k + \omega_2^k}{s - (\omega_1^k + \omega_2^k)^2 + i\epsilon} V_{fk}(\mathbf{p}, \mathbf{q}_k; s) T_{ki}(\mathbf{q}_k, \mathbf{p}'; s). \quad (4)$$

To investigate dynamically generated resonances with specific quantum numbers, we need to perform the partial-wave decomposition of the transition amplitudes as follows:

$$T_{\lambda'\lambda}^{J(fi)}(\mathbf{p}, \mathbf{p}'; s) = V_{\lambda'\lambda}^{J(fi)}(\mathbf{p}, \mathbf{p}'; s) + \sum_{k, \{\lambda_k\}} \frac{1}{(2\pi)^3} \int_0^\infty dq_k \frac{\omega_1^k + \omega_2^k}{2\omega_1^k \omega_2^k} \frac{q_k^2 V_{\lambda'\lambda_k}^{J(fk)}(\mathbf{p}, \mathbf{q}_k; s) T_{\lambda_k\lambda}^{J(ki)}(\mathbf{q}_k, \mathbf{p}'; s)}{s - (\omega_1^k + \omega_2^k)^2 + i\epsilon}, \quad (5)$$

where  $\{\lambda_k\}$  stands for the helicity components for the particles involved in the intermediate hadron channel  $k$ . The partial-wave kernel and transition amplitudes in the helicity basis are derived as

$$V_{\lambda'\lambda}^{J(fi)}(\mathbf{p}, \mathbf{p}'; s) = 2\pi \int d\cos\theta V_{fi}(\mathbf{p}, \mathbf{p}', \theta; s) d_{\lambda'\lambda}^J(\theta), \quad (6)$$

$$T_{\lambda'\lambda}^{J(fi)}(\mathbf{p}, \mathbf{p}'; s) = 2\pi \int d\cos\theta T_{fi}(\mathbf{p}, \mathbf{p}', \theta; s) d_{\lambda'\lambda}^J(\theta), \quad (7)$$

where  $d_{\lambda'\lambda}^J$  denotes the reduced Wigner  $D$  function as a function of the scattering angle  $\theta$ .  $\lambda^{(\cdot)}$  indicates the helicity difference between two particles in the initial (final) state.  $\mathbf{p}$ ,  $\mathbf{p}'$ , and  $\mathbf{q}_k$  are the magnitudes of three-momenta for initial, final, and intermediate states, respectively.

To solve the coupled integral equation (5), we first construct the kernel matrix  $V_{fi}$  based on the effective Lagrangians [32–34] with heavy-quark spin-flavor symmetry and chiral symmetry, given as

$$\mathcal{L}_{\text{heavy}}^Q = ig\text{Tr}[H_b^Q \gamma_\mu \gamma_5 \mathcal{A}_{ba}^\mu \bar{H}_a^Q] + i\beta\text{Tr}[H_b^Q v_\mu (\mathcal{V} - \rho)_{ba}^\mu \bar{H}_a^Q] + i\lambda\text{Tr}[H_b^Q \sigma_{\mu\nu} F_{ba}^{\mu\nu} \bar{H}_a^Q] + g_\sigma \bar{H}_a^Q H_a^Q \sigma, \quad (8)$$

$$\mathcal{L}_{\text{heavy}}^{\bar{Q}} = ig\text{Tr}[\bar{H}_a^{\bar{Q}} \gamma_\mu \gamma_5 \mathcal{A}_{ab}^\mu H_b^{\bar{Q}}] - i\beta\text{Tr}[\bar{H}_a^{\bar{Q}} v_\mu (\mathcal{V} - \rho)_{ab}^\mu H_b^{\bar{Q}}] + i\lambda\text{Tr}[\bar{H}_a^{\bar{Q}} \sigma_{\mu\nu} F_{ab}^{\mu\nu} H_b^{\bar{Q}}] + g_\sigma \bar{H}_a^{\bar{Q}} H_a^{\bar{Q}} \sigma, \quad (9)$$

where  $H^Q$  and its conjugate field  $\bar{H}^Q$  represent the heavy superfields that contain a heavy quark  $Q$ , and  $H^{\bar{Q}}$  and  $\bar{H}^{\bar{Q}}$  denote those for superfields with anti-heavy quark  $\bar{Q}$ . The heavy-quark spin-flavor symmetry allows us to write down the field  $H$  in terms of the pseudoscalar and vector heavy-meson fields as follows:

$$H_a^Q = \frac{1+\not{\psi}}{2}(P_a^{*Q\mu}\gamma_\mu - P_a^Q\gamma_5),$$

$$\bar{H}_a^Q = \gamma_0 H_a^{Q\dagger} \gamma_0 = (P_a^{*Q\dagger\mu}\gamma_\mu + P_a^{Q\dagger}\gamma_5) \frac{1+\not{\psi}}{2}, \quad (10)$$

$$H_a^{\bar{Q}} = (P_a^{*\bar{Q}\mu}\gamma_\mu - P_a^{\bar{Q}\mu}\gamma_5) \frac{1-\not{\psi}}{2},$$

$$\bar{H}_a^{\bar{Q}} = \gamma^0 H_a^{\bar{Q}\dagger} \gamma^0 = \frac{1-\not{\psi}}{2} [\not{P}_a^{*\bar{Q}} + P_a^{\bar{Q}}\gamma_5], \quad (11)$$

where  $P^Q$  and  $P^{*Q}$  stand for the heavy meson antitriplet in flavor SU(3) symmetry with a heavy quark  $Q$  regarded as the static color source. These fields are normalized by

$$\langle 0|P|D(B)\rangle = \sqrt{M_{D(B)}}, \quad (12)$$

$$\langle 0|P^{*\mu}|D^*(B^*)\rangle = \epsilon^\mu \sqrt{M_{D^*(B^*)}}, \quad (13)$$

where  $\epsilon^\mu$  designates the polarization vector of the heavy vector meson. The SU(3) triplet field  $P^{\bar{Q}}$  and  $P^{*\bar{Q}}$  are also defined in the same manner. The interactions of the pseudo-Nambu-Goldstone (pNG) bosons with the matter field  $H$  can be derived by the non-linear realization of the pNG fields. The coset field  $\xi(x)$ , which arises from spontaneous breakdown of chiral symmetry, is parametrized in the coset space  $\text{SU}(3)_L \otimes \text{SU}(3)_R / \text{SU}(3)_V$  as  $\xi(x) = \exp(i\mathcal{M}/f_\pi)$  with the pion decay constant  $f_\pi = 132$  MeV taken as a normalization factor. Here the  $\mathcal{M}$  represents the matrix in flavor space that describes the SU(3) pNG fields or the light pseudoscalar meson matrix:

$$\mathcal{M} = \begin{pmatrix} \frac{\pi^0}{\sqrt{2}} + \frac{\eta}{\sqrt{6}} & \pi^+ & K^+ \\ \pi^- & -\frac{\pi^0}{\sqrt{2}} + \frac{\eta}{\sqrt{6}} & K^0 \\ K^- & \bar{K}^0 & -\sqrt{\frac{2}{3}}\eta \end{pmatrix}. \quad (14)$$

One can introduce the axial-vector and vector currents:

$$\mathcal{A}^\mu = \frac{1}{2}(\xi^\dagger \partial^\mu \xi - \xi \partial^\mu \xi^\dagger), \quad (15)$$

$$\mathcal{V}^\mu = \frac{1}{2}(\xi^\dagger \partial^\mu \xi + \xi \partial^\mu \xi^\dagger), \quad (16)$$

and the axial-vector current can be expanded as:

$$\mathcal{A}^\mu = \frac{1}{2}(\xi^\dagger \partial^\mu \xi - \xi \partial^\mu \xi^\dagger) = \frac{i}{f_\pi} \partial^\mu \mathcal{M} + \dots \quad (17)$$

It indicates that the derivative coupling is natural for the light pseudoscalar meson and heavy mesons on account of chiral symmetry and its spontaneous breakdown.

The effective Lagrangian for the vector meson octet is constructed by means of the hidden local symmetry approach. Bando et al. [32, 35] suggested the gauge equivalence between  $\text{SU}(3)_L \otimes \text{SU}(3)_R / \text{SU}(3)_V$  and  $[\text{SU}(3)_L \otimes \text{SU}(3)_R] \otimes [\text{SU}(3)_V]_{\text{local}}$ , where  $[\text{SU}(3)_V]_{\text{local}}$  stands for the hidden local symmetry and the dynamical gauge bosons appear as the composite fields. The invariance under the local symmetry requires the new interaction terms in the effective Lagrangian corresponding to the third and fourth term in Eq. (9). The vector meson octet is then expressed as:

$$\rho^\mu = i \frac{g_V}{\sqrt{2}} V^\mu, \quad V^\mu = \begin{pmatrix} \frac{\rho^0}{\sqrt{2}} + \frac{\omega}{\sqrt{6}} & \rho^+ & K^{*+} \\ \rho^- & -\frac{\rho^0}{\sqrt{2}} + \frac{\omega}{\sqrt{6}} & K^{*0} \\ K^{*-} & \bar{K}^{*0} & -\sqrt{\frac{2}{3}}\omega \end{pmatrix}^\mu, \quad (18)$$

with the field strength tensor  $F^{\mu\nu} = \partial^\mu \rho^\nu - \partial^\nu \rho^\mu + [\rho^\mu, \rho^\nu]$ .

The expansion of the effective Lagrangian in Eq. (9) represents the interaction terms for  $P^{Q(\bar{Q})}$ ,  $P^{*Q(\bar{Q})}$ ,  $\mathcal{M}$ , and  $V$ . The first term of Eq. (1) gives the effective Lagrangians for  $PP^*\mathcal{M}$  and  $P^*P^*\mathcal{M}$  vertices:

$$\mathcal{L}_{P^Q P^*Q \mathcal{M}} = -\frac{2g}{f_\pi} P_b^{*Q\mu} \partial_\mu \mathcal{M}_{ba} P_a^{Q\dagger} + \text{h.c.}, \quad (19)$$

$$\mathcal{L}_{P^*Q P^*Q \mathcal{M}} = \frac{2ig}{f_\pi} P_b^{*Q\beta} \partial^\mu \mathcal{M}_{ba} v^\nu P_a^{*Q\alpha\dagger} \varepsilon_{\alpha\beta\mu\nu} + \text{h.c.}, \quad (20)$$

$$\mathcal{L}_{P^{\bar{Q}} P^*\bar{Q} \mathcal{M}} = \frac{2g}{f_\pi} P_b^{*\bar{Q}\mu} \partial_\mu \mathcal{M}_{ba} P_a^{\bar{Q}\dagger} + \text{h.c.}, \quad (21)$$

$$\mathcal{L}_{P^*\bar{Q} P^*\bar{Q} \mathcal{M}} = \frac{2ig}{f_\pi} P_b^{*\bar{Q}\beta} \partial^\mu \mathcal{M}_{ba} v^\nu P_a^{*\bar{Q}\alpha\dagger} \varepsilon_{\alpha\beta\mu\nu} + \text{h.c.}. \quad (22)$$

The interactions of  $PPV$ ,  $PP^*V$ , and  $P^*P^*V$  then come from the second and third terms of Eq. (9):

$$\begin{aligned} \mathcal{L}_{P^Q P^Q V} &= -2i\beta P^Q P^{Q\dagger} v \cdot \rho \\ &= -\sqrt{2}\beta g_V P^Q P^{Q\dagger} v \cdot V, \end{aligned} \quad (23)$$

$$\begin{aligned} \mathcal{L}_{P^Q P^*Q V} &= -4i\lambda \varepsilon_{\mu\nu\alpha\beta} (P^Q \partial^\mu P^{*Q\dagger\nu} + P^{Q\dagger} \partial^\mu P^{*Q\nu}) v^\alpha \rho^\beta \\ &= 2\sqrt{2}\lambda g_V \varepsilon_{\mu\nu\alpha\beta} (P^Q \partial^\mu P^{*Q\dagger\nu} + P^{Q\dagger} \partial^\mu P^{*Q\nu}) v^\alpha V^\beta, \end{aligned} \quad (24)$$

$$\begin{aligned} \mathcal{L}_{P^*Q P^*Q V} &= -2i\beta P^{*Q\mu} P_\mu^{*Q\dagger} v \cdot \rho - 4\lambda (\partial_\mu P^{*Q\dagger\mu} P_\nu^{*Q} - \partial_\mu P^{*Q\mu} P_\nu^{*Q\dagger}) \rho^\nu \\ &= \sqrt{2}\beta g_V P^{*Q\mu} P_\mu^{*Q\dagger} v \cdot V - 2\sqrt{2}i\lambda g_V (\partial_\mu P^{*Q\dagger\mu} P_\nu^{*Q} - \partial_\mu P^{*Q\mu} P_\nu^{*Q\dagger}) V^\nu, \end{aligned} \quad (25)$$

$$\begin{aligned} \mathcal{L}_{P^{\bar{Q}} P^{\bar{Q}} V} &= 2i\beta P^{\bar{Q}} P^{\bar{Q}\dagger} v \cdot \rho \\ &= \sqrt{2}\beta g_V P^{\bar{Q}} P^{\bar{Q}\dagger} v \cdot V, \end{aligned} \quad (26)$$

$$\begin{aligned} \mathcal{L}_{P^{\bar{Q}} P^*\bar{Q} V} &= -4i\lambda \varepsilon_{\mu\nu\alpha\beta} (P^{\bar{Q}} \partial^\mu P^{*\bar{Q}\dagger\nu} + P^{*\bar{Q}\dagger} \partial^\mu P^{*\bar{Q}\nu}) v^\alpha \rho^\beta \\ &= 2\sqrt{2}\lambda g_V \varepsilon_{\mu\nu\alpha\beta} (P^{\bar{Q}} \partial^\mu P^{*\bar{Q}\dagger\nu} + P^{*\bar{Q}\dagger} \partial^\mu P^{*\bar{Q}\nu}) v^\alpha V^\beta, \end{aligned} \quad (27)$$

$$\begin{aligned} \mathcal{L}_{P^*\bar{Q} P^*\bar{Q} V} &= -2i\beta P^{*\bar{Q}\mu} P_\mu^{*\bar{Q}\dagger} v \cdot \rho + 4\lambda (\partial_\mu P^{*\bar{Q}\dagger\mu} P_\nu^{*\bar{Q}} - \partial_\mu P^{*\bar{Q}\mu} P_\nu^{*\bar{Q}\dagger}) \rho^\nu \\ &= \sqrt{2}\beta g_V P^{*\bar{Q}\mu} P_\mu^{*\bar{Q}\dagger} v \cdot V + 2\sqrt{2}i\lambda g_V (\partial_\mu P^{*\bar{Q}\dagger\mu} P_\nu^{*\bar{Q}} - \partial_\mu P^{*\bar{Q}\mu} P_\nu^{*\bar{Q}\dagger}) V^\nu. \end{aligned} \quad (28)$$

The effective Lagrangians for interaction with the scalar meson  $\sigma$  are obtained as:

$$\mathcal{L}_{P^Q P^Q \sigma} = -2g_{P^Q P^Q \sigma} P_a^{Q\dagger} P_a^Q \sigma, \quad (29)$$

$$\mathcal{L}_{P^*Q P^*Q \sigma} = 2g_{P^*Q P^*Q \sigma} P_{a\mu}^{*Q\dagger} P_a^{*Q\mu} \sigma, \quad (30)$$

$$\mathcal{L}_{P^{\bar{Q}} P^{\bar{Q}} \sigma} = -2g_{P^{\bar{Q}} P^{\bar{Q}} \sigma} P_a^{\bar{Q}\dagger} P_a^{\bar{Q}} \sigma, \quad (31)$$

$$\mathcal{L}_{P^*\bar{Q} P^*\bar{Q} \sigma} = 2g_{P^*\bar{Q} P^*\bar{Q} \sigma} P_{a\mu}^{*\bar{Q}\dagger} P_a^{*\bar{Q}\mu} \sigma, \quad (32)$$

where the heavy quark velocity can be replaced by  $i \overleftrightarrow{\partial}_\mu / (2\sqrt{MM'}) = i(\overleftarrow{\partial} - \overrightarrow{\partial}) / (2\sqrt{MM'})$ , with  $M^{(\prime)}$  denoting the mass of the heavy meson.

Charmonia and light unflavored mesons can be involved in the energy region, where hidden-charm exotic mesons are dynamically generated. The corresponding effective Lagrangian is given by:

$$\mathcal{L}_J = g_\psi \text{Tr}[J \bar{H}_a^{\bar{Q}} \gamma_\mu \partial^\mu \bar{H}_a^Q], \quad (33)$$

where  $J$  represents the charmonium superfield containing both pseudoscalar ( $\eta_c$ ) and vector ( $J/\psi$ ) components:

$$J = \frac{1+\not{v}}{2} [\psi^\mu \gamma_\mu - \eta_c \gamma_5] \frac{1-\not{v}}{2}. \quad (34)$$

We get the corresponding effective Lagrangian for the pseudoscalar charmonium  $\eta_c$ :

$$\mathcal{L}_{\eta_c} = -g_\psi \eta_c (P^{\bar{Q}\dagger} v \cdot P^{*Q\dagger} + P^{Q\dagger} v \cdot P^{*\bar{Q}\dagger}) - ig_\psi \eta_c \varepsilon_{\beta\alpha\mu\nu} P^{*\bar{Q}\alpha\dagger} v^\beta P^{*Q\dagger\mu} v^\nu, \quad (35)$$

and for the vector charmonium  $J/\psi$  ( $\psi^\mu$ ):

$$\begin{aligned} \mathcal{L}_{J/\psi} = & ig_\psi \varepsilon^{\beta\alpha\mu\nu} v_\nu \psi_\alpha \left( P^{Q\dagger} v_\beta P_\mu^{*\bar{Q}\dagger} + P_\beta^{*Q\dagger} v_\alpha P^{Q\dagger} \right) + \psi_\mu P_\nu^{*Q\dagger} v_\alpha P_\beta^{*\bar{Q}\dagger} (g^{\mu\nu} g^{\alpha\beta} - g^{\mu\alpha} g^{\nu\beta} + g^{\mu\beta} g^{\nu\alpha}) \\ & - g_\psi P^{Q\dagger} v \cdot \psi P^{Q\dagger}. \end{aligned} \quad (36)$$

We now discuss how the values of the coupling constants in Eq. (9) can be determined.  $g$  is the axial coupling constant and its value is extracted to be  $g = 0.59$  from the  $D^* \rightarrow D\pi$  decay rate [36]:

$$\Gamma(D^{*+} \rightarrow D^0\pi^+) = \frac{g^2}{6\pi f_\pi^2} |\mathbf{p}_\pi|^3, \quad (37)$$

The interactions of  $PPV$ ,  $PP^*V$ , and  $P^*P^*V$  then come from the second and third terms of Eq. (9).  $\beta = 0.9$  is determined by the vector meson dominance [35]. The value of  $\lambda = 0.56 \text{ GeV}^{-1}$  is taken from Ref. [37], which is the coupling constant for the third term given in Eq. (9). Note that it is related to the  $PP^*V$  vertex and  $P^*P^*V$  tensor coupling. The value of  $\lambda$  can be determined from the  $B \rightarrow K^*$  vector transition form factor at very high  $q^2$  based on the effective field theory approach. With the results from the light-cone QCD sum rules and lattice QCD matched, its value is set to be  $\lambda = 0.56 \text{ GeV}^{-1}$ . The  $\sigma$  state (also known as  $f(500)$ ) in Eq. (32) is often regarded as a chiral partner of the pion, so that the following relation was suggested:  $g_\sigma = g_\pi/(2\sqrt{6})$ . In Ref. [38], however, the large width of the  $\sigma$  from dynamics of the correlated  $2\pi$  exchange were considered and the values of  $g_{DD\sigma} = 1.50$  and  $g_{D^*D^*\sigma} = 5.21$  were extracted by using the dispersion relation. The  $g_{DD\rho} = 1.65$  and  $g_{D^*D^*\rho} = 6.47$  were also obtained in the same manner by analyzing the vector-isovector  $2\pi$ -correlated exchange. The  $g_{DD^*\rho}$  coupling constant is fixed by using the KSFRF relation [39, 40]:  $g_{DD^*\rho} = 5.8$ .

We now construct the kernel matrix for charmonium-like states,  $\chi_{cJ}$  and  $\psi_J$ , within the energy range of the  $D\bar{D}$ ,  $D\bar{D}^*$ , and  $D^*\bar{D}^*$  thresholds. We are able to list the two-hadron state with  $I = 0$  lying near these thresholds as follows:

- $D\bar{D}$ ,  $D\bar{D}^*$ ,  $D^*\bar{D}^*$ ,  $D_s\bar{D}_s$ ,  $D_s\bar{D}_s^*$ ,  $D_s^*\bar{D}_s^*$  ( $G = \pm 1$ ),
- $J/\psi\omega$ ,  $J/\psi\phi$ , ( $G = +1$ )
- $\eta_c\omega$ ,  $\eta_c\phi$ , ( $G = -1$ )

To properly define the allowed hadronic channels for the  $\chi_{cJ}$  and  $\psi_J$  families, we must classify the two-body states according to their exact quantum numbers. Since our scope is restricted to the isoscalar sector ( $I = 0$ ), the  $G$ -parity is equivalent to the charge-conjugation parity,  $G = C(-1)^I = C$ . Furthermore, because the constituent mesons in the present study are either pseudoscalar ( $J^P = 0^-$ ) or vector ( $J^P = 1^-$ ), the intrinsic parity of any two-meson channel is always positive ( $P_1P_2 = (-1)^2 = +1$ ). Consequently, the total parity of the system is determined entirely by the relative orbital angular momentum  $L$ , yielding  $P = (-1)^L$ .

The assignment of  $C$ -parity requires careful treatment depending on the nature of the interacting mesons. For hidden-charm channels consisting of a charmonium and a light vector meson (such as  $J/\psi\omega$  and  $\eta_c\phi$ ), the total  $C$ -parity is simply the product of the intrinsic  $C$ -parities of the constituents,  $C = C_1C_2$ , completely independent of the relative orbital angular momentum. For open-flavor channels composed of identical meson-antimeson pairs (such as  $D\bar{D}$  and  $D^*\bar{D}^*$ ), the  $C$ -parity depends on both the orbital angular momentum  $L$  and the total spin  $S$  of the two-meson system, given by  $C = (-1)^{L+S}$ .

On the other hand, non-identical open-flavor meson pairs, such as  $D\bar{D}^*$ , are not  $C$ -eigenstates. The  $C$ -parity eigenstates are constructed via symmetric or antisymmetric linear combinations:

$$|D\bar{D}^*\rangle_{C=\pm} = \frac{1}{\sqrt{2}} (|D\bar{D}^*\rangle \mp |\bar{D}D^*\rangle), \quad (38)$$

with  $C|D(\bar{D})\rangle = +|D(\bar{D})\rangle$  and  $C|D^*(\bar{D}^*)\rangle = -|D^*(\bar{D}^*)\rangle$ . By imposing these exact selection rules, we systematically construct two independent kernel matrices composed of the relevant hadronic channels for the positive- $G$ -parity ( $\chi_{cJ}$ ) and negative- $G$ -parity ( $\psi_J$ ) sectors.

The kernel matrix element is written as the sum of tree-level Feynman amplitudes for all allowed single-meson exchanges,

$$\mathcal{V}_{i \rightarrow j} = \sum_A \mathcal{M}_{i \rightarrow j}^A, \quad (39)$$

where  $A$  labels the exchanged particle in the process  $i \rightarrow j$ . As mentioned in the Introduction, we have intentionally excluded any  $s$ -channel contributions in this study, since we focus on the resonances generated by the coupled-channel

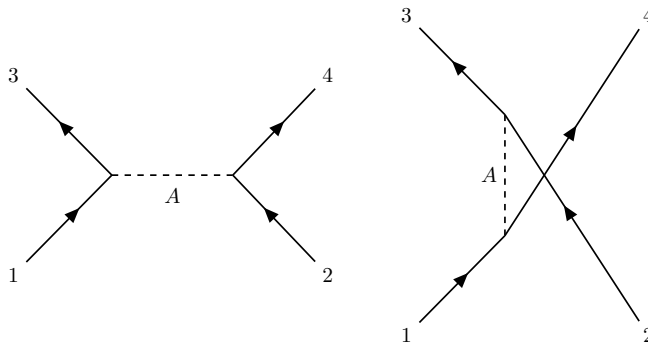


FIG. 3.  $t$ - and  $u$ -channel Feynman diagrams for  $12 \rightarrow 34$ .

formalism. Figure 3 shows a generic tree-level diagram with two vertices and a meson propagator. The Feynman amplitudes for the exchange of  $A$  read

$$\begin{aligned} \mathcal{M}_{12 \rightarrow 34}^A(t) &= \text{IS} F_A^2 \Gamma_{13}^A P^A \Gamma_{24}^A, \\ \mathcal{M}_{12 \rightarrow 34}^A(u) &= \text{IS} F_A^2 \Gamma_{14}^A P^A \Gamma_{23}^A, \end{aligned} \quad (40)$$

where  $\Gamma_{ij}^A$  denotes the vertex function that couples the  $i$  and  $j$  legs to the exchanged particle  $A$ . The vertex functions are obtained straightforwardly from the effective Lagrangians in Eqs. (22)–(32) and (37). The quantity  $P^A$  is the propagator of the exchanged particle  $A$ . The propagators for spin-0 and spin-1 particles are given by

$$P^A(q) = \frac{1}{q^2 - m_A^2}, \quad P_{\mu\nu}^A(q) = \frac{-g_{\mu\nu} + \frac{q_\mu q_\nu}{m_A^2}}{q^2 - m_A^2}. \quad (41)$$

The factor IS denotes the isospin factor arising from the isospin projector and SU(3) Clebsch–Gordan coefficients.

We introduce a form factor at each vertex, since hadrons have finite sizes. This form factor is also necessary to ensure the unitarity of the transition amplitudes. We use the following form [41]:

$$F(q^2) = \left( \frac{n\Lambda^2 - m_A^2}{n\Lambda^2 - q^2} \right)^n, \quad (42)$$

where the value of  $n$  depends on the momentum power present in the vertex function  $\Gamma$ . Note that we have turned off the energy dependence in Eq. (42), which causes unphysical behaviors of the kernel amplitudes. Although there is no experimental information on the values of the cutoff masses  $\Lambda$  in Eq. (42), one can reduce the uncertainties associated with them by considering physical properties of the hadrons involved. Investigations of the electromagnetic form factors of singly heavy baryons [42, 43] have shown that sizes of heavy hadrons are more compact than those of lighter ones. This implies that higher cutoff masses are more suitable for heavy hadrons than for light ones, since the value of the cutoff mass is proportional to the inverse of the size of the corresponding hadron. Thus, we define the reduced cutoff mass as  $\Lambda_0 := \Lambda - m_A$ . Interestingly, in Ref. [44], the cutoff mass is related to  $\Lambda_{\text{QCD}}$  via  $\Lambda = m + \eta\Lambda_{\text{QCD}}$ , where  $\eta$  is of order unity. This method has been successfully applied in previous works [21–24, 26–28, 45]. In the present study, we fix the values of the reduced cutoff to be  $\Lambda_0 = 600$  MeV for all vertices throughout the calculation. We emphasize that no fitting procedure is employed in the present study. The values of the isospin factors IS and the adopted  $\Lambda_0$  for the isoscalar and isovector sectors are listed in Tables I and II, respectively.

### III. RESULTS AND DISCUSSION

We are now in a position to present the numerical results and to discuss them. We focus on the dynamical generation of bound states and resonances in the transition amplitudes in the hidden-charm sector over 3.6 to 4.3 GeV. Since the partial-wave decomposition is most conveniently performed in the helicity basis using the Wigner  $d$ -functions, the transition amplitudes are first obtained by solving the coupled-channel integral equation (5) in the helicity basis and subsequently transformed to the  $LSJ$  basis, which allows us to analyze resonant behavior with definite spin, orbital, and total angular momentum. In addition to parity, we impose charge conjugation and  $G$  parity, and classify states by  $I^G(J^{PC})$ . In the charmonium sector, four families are in principle relevant:  $\chi_{cJ}$  with  $J^{++}$ ,  $\psi_J$  with  $J^{--}$ ,  $\eta_c$  with  $J^{-+}$ ,

TABLE I. The values of the SU(3) symmetric factor for the transitions between open-flavor channels and isospin factor for the kernel amplitude in isoscalar ( $I = 0$ ) channel.  $\Lambda_0$  denotes the reduced cutoff mass defined as  $\Lambda - m_{\text{ex}}$ .

Reaction	Exchange	IS factor		$\Lambda_0$ [MeV]
		$t$ -ch	$u$ -ch	
$D\bar{D} \rightarrow D\bar{D}$	$\sigma$	1	-1	600
	$\rho$	3/2	-3/2	600
	$\omega$	1/2	-1/2	600
$D\bar{D} \rightarrow D\bar{D}^*$	$\rho$	3/2	-3/2	600
	$\omega$	1/2	-1/2	600
$D\bar{D} \rightarrow D_s\bar{D}_s$	$K^*$	$-\sqrt{2}$	$-\sqrt{2}$	600
$D\bar{D} \rightarrow D_s\bar{D}_s^*$	$K^*$	$-\sqrt{2}$	$-\sqrt{2}$	600
$D\bar{D} \rightarrow D^*\bar{D}^*$	$\pi, \rho$	3/2	-3/2	600
	$\eta$	1/6	-1/6	600
	$\omega$	1/2	-1/2	600
$D\bar{D} \rightarrow D_s^*\bar{D}_s^*$	$K, K^*$	$-\sqrt{2}$	$-\sqrt{2}$	600
$D\bar{D}^* \rightarrow D\bar{D}^*$	$\sigma$	1	-	600
	$\pi$	-	-3/2	600
	$\eta$	-	1/6	600
	$\rho$	3/2	-3/2	600
	$\omega$	1/2	-1/2	600
$D\bar{D}^* \rightarrow D_s\bar{D}_s$	$K^*$	$-\sqrt{2}$	$-\sqrt{2}$	600
$D\bar{D}^* \rightarrow D^*\bar{D}^*$	$\pi, \rho$	3/2	-3/2	600
	$\eta$	1/6	-1/6	600
	$\omega$	1/2	-1/2	600
$D\bar{D}^* \rightarrow D_s\bar{D}_s^*$	$K$	-	$-\sqrt{2}$	600
	$K^*$	$-\sqrt{2}$	$-\sqrt{2}$	600
$D\bar{D}^* \rightarrow D_s^*\bar{D}_s^*$	$K, K^*$	$-\sqrt{2}$	$-\sqrt{2}$	600
$D_s\bar{D}_s \rightarrow D_s\bar{D}_s$	$\sigma, \phi$	1	1	600
$D_s\bar{D}_s \rightarrow D^*\bar{D}^*$	$K, K^*$	$-\sqrt{2}$	$-\sqrt{2}$	600
$D_s\bar{D}_s \rightarrow D_s\bar{D}_s^*$	$\phi$	1	1	600
$D_s\bar{D}_s \rightarrow D_s^*\bar{D}_s^*$	$\eta$	2/3	2/3	600
	$\phi$	1	1	600
$D^*\bar{D}^* \rightarrow D^*\bar{D}^*$	$\sigma$	1	-1	600
	$\pi, \rho$	3/2	-3/2	600
	$\eta$	1/6	-1/6	600
	$\omega$	1/2	-1/2	600
$D^*\bar{D}^* \rightarrow D_s\bar{D}_s^*$	$K, K^*$	$-\sqrt{2}$	$-\sqrt{2}$	600
$D^*\bar{D}^* \rightarrow D_s^*\bar{D}_s^*$	$K, K^*$	$-\sqrt{2}$	$-\sqrt{2}$	600
$D_s\bar{D}_s^* \rightarrow D_s\bar{D}_s^*$	$\sigma$	1	-	600
	$\eta$	-	2/3	600
	$\phi$	1	1	600
$D_s\bar{D}_s^* \rightarrow D_s^*\bar{D}_s^*$	$\eta$	2/3	2/3	600
	$\phi$	1	1	600
$D_s^*\bar{D}_s^* \rightarrow D_s^*\bar{D}_s^*$	$\sigma, \phi$	1	1	600
	$\eta$	2/3	2/3	600

TABLE II. The values of the SU(3) symmetric factor with the channels containing a charmonium and isospin factor for the kernel amplitude in isoscalar ( $I = 0$ ) channel.  $\Lambda_0$  denotes the reduced cutoff mass defined as  $\Lambda - m_{\text{ex}}$ .

Reaction	Exchange	IS factor		$\Lambda_0$ [MeV]
		$t$ -ch	$u$ -ch	
$\omega\eta_c \rightarrow D\bar{D}$	$D^*$	-1	-1	600
$\omega\eta_c \rightarrow D\bar{D}^*$	$D, D^*$	-1	-1	600
$\omega\eta_c \rightarrow D^*\bar{D}^*$	$D, D^*$	-1	-1	600
$\phi\eta_c \rightarrow D_s\bar{D}_s$	$D_s^*$	$-\sqrt{2}$	$-\sqrt{2}$	600
$\phi\eta_c \rightarrow D_s\bar{D}_s^*$	$D_s, D_s^*$	$-\sqrt{2}$	$-\sqrt{2}$	600
$\phi\eta_c \rightarrow D_s^*\bar{D}_s^*$	$D_s, D_s^*$	$-\sqrt{2}$	$-\sqrt{2}$	600
$\omega J/\psi \rightarrow D\bar{D}$	$D, D^*$	-1	-1	600
$\omega J/\psi \rightarrow D\bar{D}^*$	$D, D^*$	-1	-1	600
$\omega J/\psi \rightarrow D^*\bar{D}^*$	$D, D^*$	-1	-1	600
$\phi J/\psi \rightarrow D_s\bar{D}_s^*$	$D_s, D_s^*$	$-\sqrt{2}$	$-\sqrt{2}$	600
$\phi J/\psi \rightarrow D_s\bar{D}_s$	$D_s, D_s^*$	$-\sqrt{2}$	$-\sqrt{2}$	600
$\phi J/\psi \rightarrow D_s^*\bar{D}_s^*$	$D_s, D_s^*$	$-\sqrt{2}$	$-\sqrt{2}$	600

and  $h_c$  with  $J^{+-}$ . Since most experimentally reported excited  $c\bar{c}$  states fall into the  $\chi_{cJ}$  and  $\psi_J$  families, we restrict our analysis to these two sectors. We scan the transition amplitudes extended into the complex energy plane and search for poles with the quantum numbers  $I^G(J^{PC})$  generated dynamically by the corresponding coupled-channel reactions. The coupling strength to each hadronic channel is then extracted from the residues of the poles, providing information on the nature of the bound or resonance states.

### A. $\chi_{cJ}$ states: $I^G(J^{PC}) = 0^+(J^{++})$

#### 1. $\chi_{c0}$ $J^{PC} = 0^{++}$

Figure 4 shows the diagonal transition amplitudes for  $\chi_{c0}$  states in the  $^1S_0$  partial wave near open-flavor thresholds. Note that charmonium channels do not appear as diagonal entries in Fig. 4, since they do not contribute to elastic scattering in this partial wave. We find two pole structures in this channel. The first is a bound state just below the  $D\bar{D}$  threshold, generated primarily by elastic  $D\bar{D}$  scattering, as signaled by the sharp variation of the  $D\bar{D}$  amplitude near  $\sqrt{s} \approx 3720$  MeV in Fig. 4. When all six hadronic channels listed in Table I are coupled, the pole is found at  $\sqrt{s_R} = 3720.5$  MeV, corresponding to a binding energy of 14 MeV. Experimentally, however, no bound state with  $J^{PC} = 0^{++}$  below the  $D\bar{D}$  threshold has been established. The second is a clear resonance between the  $D\bar{D}$  and  $J/\psi\omega$  thresholds, with pole position  $\sqrt{s_R} = (3861.34 - i22.76)$  MeV. As can be seen in Fig. 4, the most pronounced structure in the transition amplitude appears in the  $D^*\bar{D}^*$  channel near  $\sqrt{s} \approx 3900$  MeV, indicating that the dynamical generation of this resonance is driven primarily by the  $D^*\bar{D}^*$  channel, even though the pole is positioned near the  $J/\psi\omega$  threshold. We call this pole a  $\chi_{c0}(3861)$ -like state. Above the  $D_s\bar{D}_s$  threshold we do not find any further peak structure in this channel. The identification of this state with known experimental candidates is not straightforward, since there is still debate over the  $\chi_{c0}(2P)$  assignment between  $\chi_{c0}(3860)$  and  $\chi_{c0}(3915)$ , both of which were observed in the  $D\bar{D}$  mode. The reported pole positions are  $E_{\text{pole}}(\chi_{c0}(3860)) = (3862_{-35}^{+50} - i200_{-110}^{+180})$  MeV and  $E_{\text{pole}}(\chi_{c0}(3915)) = (3922.1 \pm 1.8 - i20 \pm 4)$  MeV. In mass our pole is closer to  $\chi_{c0}(3860)$ , while in width it is closer to  $\chi_{c0}(3915)$ .

For a quantitative analysis of coupled-channel effects, we extract the coupling strength to each channel by parametrizing the transition matrix near  $\sqrt{s_R}$  with a Breit-Wigner form,

$$T_{a \rightarrow a}(\sqrt{s}) = 4\pi \frac{g_a^2}{s - s_R}, \quad (43)$$

where the residue  $g_a$  is the coupling strength for channel  $a$ . The results are listed in Table III. The bound state below the  $D\bar{D}$  threshold couples dominantly to  $D\bar{D}$ , with a subleading coupling to  $D_s\bar{D}_s$ , both in  $S$  wave. The resonance

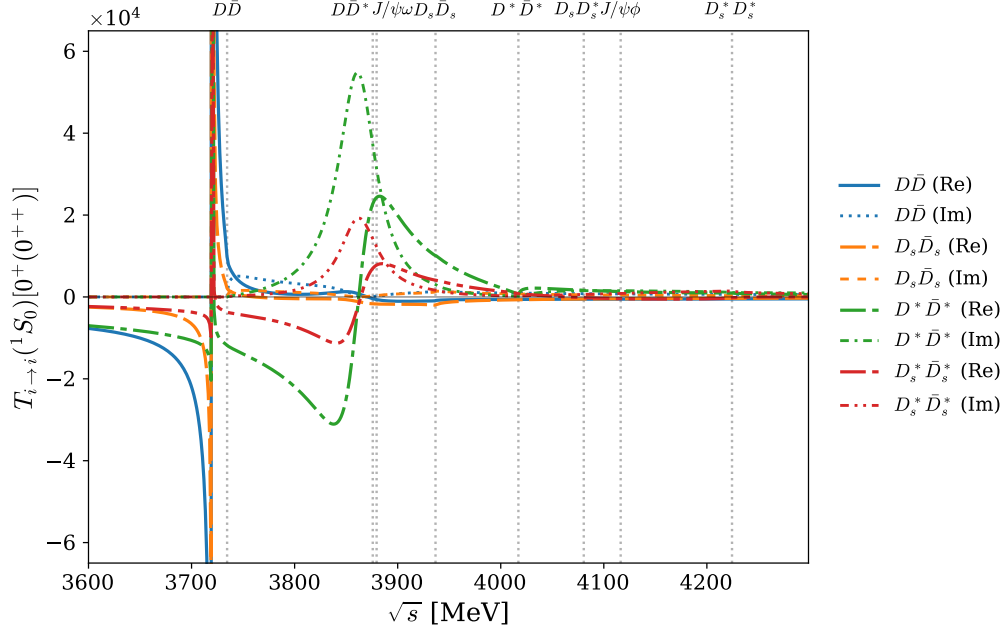


FIG. 4. Diagonal partial-wave transition amplitudes for the  $I^G(J^{PC}) = 0^+(0^{++})$  channel as functions of  $\sqrt{s}$ .

at  $(3861.34 - i22.76)$  MeV couples strongly to  $D^*\bar{D}^*$ , and the coupling to  $D_s^*\bar{D}_s^*$  is also large, consistent with strong vector-meson exchange attraction in  $S$  wave. Indeed, this resonance originates as a deep bound state in the  $D^*\bar{D}^*$  channel and is shifted upward by coupled-channel dynamics, driven predominantly by the  $D_s^*\bar{D}_s^*$  channel.

TABLE III. Coupling strengths  $g_i$  for the  $^1S_0$  states (in GeV). Higher partial wave contributions are omitted as they are negligible. Values in parentheses denote  $|g_i|$ .

$\sqrt{s_R}$ [MeV]	3720.5	3861.34 - i22.76
$g_{D\bar{D}}(^1S_0)$	14.13	$5.547 + i5.774$ (8.007)
$g_{J/\psi\omega}(^1S_0)$	0.190	$0.561 - i0.099$ (0.570)
$g_{D_s\bar{D}_s}(^1S_0)$	7.484	$2.272 + i4.924$ (5.423)
$g_{D^*\bar{D}^*}(^1S_0)$	2.680	$36.41 - i16.022$ (39.78)
$g_{J/\psi\phi}(^1S_0)$	0.178	$0.482 - i0.074$ (0.488)
$g_{D_s^*\bar{D}_s^*}(^1S_0)$	2.228	$20.89 - i10.769$ (23.51)

## 2. $\chi_{c1} J^{PC} = 1^{++}$

Figure 5 shows the transition amplitudes for  $\chi_{c1}$  states near open-charm thresholds in the  $1^{++}(^3S_1)$  channel. We find two pole structures in this channel. The first is a bound state at  $\sqrt{s_R} = 3874.26$  MeV, lying almost exactly at the  $D\bar{D}^*$  threshold. As can be seen in Fig. 5, the sharp variation of the  $D\bar{D}^*$  amplitude near this energy confirms that this state is generated mainly by elastic  $D\bar{D}^*$  scattering in  $S$  wave, making it a natural candidate for the well-known  $\chi_{c1}(3872)$ . The second is a broader resonance above the  $D\bar{D}^*$  threshold at  $\sqrt{s_R} = (3961.40 - i32.25)$  MeV, whose extracted pole position suggests a possible identification with the  $X(3940)$ , observed in the  $D\bar{D}^*$  decay mode but not in  $D\bar{D}$  [29].

The channel couplings in Table IV clarify the dynamical origin of the two  $1^{++}$  poles. For the bound state at  $\sqrt{s_R} = 3874.26$  MeV, the largest coupling is to  $D\bar{D}^*$  and  $D_s\bar{D}_s^*$  in  $^3S_1$ . Interestingly, the couplings to  $D^*\bar{D}^*(^3S_1)$  and  $D_s^*\bar{D}_s^*(^3S_1)$  are comparable to those for  $D\bar{D}^*$  and  $D_s\bar{D}_s^*$ , indicating a nontrivial structure of the  $\chi_{c1}(3872)$  beyond a pure  $D\bar{D}^*$  molecular picture, even without invoking isospin breaking. Hidden-charm channels are small, and the

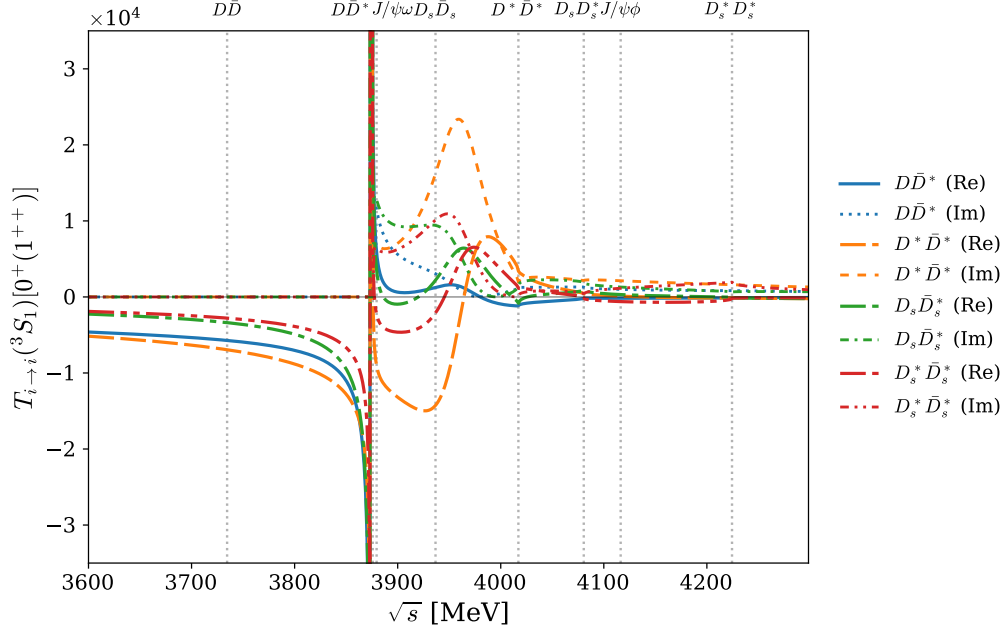


FIG. 5. Axial-vector transition amplitudes for diagonal elements as functions of  $\sqrt{s}$  for  $I^G(J^{PC}) = 0^+(1^{++})$  channel.

$D$ -wave components are essentially negligible. For the higher pole at  $\sqrt{s_R} = (3961.40 - i32.25)$  MeV, the  $S$ -wave vector-meson pair channel  $D^*\bar{D}^*(^3S_1)$  carries the dominant coupling. The  $D_s\bar{D}_s^*(^3S_1)$  and  $DD\bar{D}^*(^3S_1)$  couplings are sizable but subleading, and the  $D$ -wave components are smaller by one to two orders of magnitude than the  $S$ -wave contributions. Thus this resonance, dominated by open-flavor  $S$ -wave channels, is consistent with the broad structure of the  $X(3940)$ .

TABLE IV. Coupling strengths  $g_i$  for the  $^3S_1$  and  $^3D_1$  channels (in GeV). For the bound state at 3874.26 MeV, imaginary parts are omitted due to their negligible magnitude. Values in parentheses denote  $|g_i|$ .

$\sqrt{s_R}[\text{MeV}]$	3874.26	3961.40 - i 32.25
$g_{D\bar{D}^*}(^3S_1)$	7.125	$3.712 + i 6.796$ (7.744)
$g_{J/\psi\omega}(^3S_1)$	0.102	$0.447 + i 0.060$ (0.451)
$g_{D^*\bar{D}^*}(^3S_1)$	4.863	$22.03 + i 1.355$ (22.07)
$g_{D_s\bar{D}_s^*}(^3S_1)$	6.898	$10.73 + i 8.910$ (13.95)
$g_{J/\psi\phi}(^3S_1)$	0.018	$0.023 + i 0.044$ (0.050)
$g_{D_s^*\bar{D}_s^*}(^3S_1)$	4.657	$14.33 + i 6.075$ (15.56)
$g_{D\bar{D}^*}(^3D_1)$	0.001	$0.179 - i 1.046$ (1.061)
$g_{J/\psi\omega}(^3D_1)$	0.000	$0.023 - i 0.039$ (0.045)
$g_{D^*\bar{D}^*}(^3D_1)$	0.084	$0.140 + i 0.093$ (0.168)
$g_{D_s\bar{D}_s^*}(^3D_1)$	0.161	$0.111 + i 0.158$ (0.193)
$g_{J/\psi\phi}(^3D_1)$	0.001	$0.000 + i 0.001$ (0.001)
$g_{D_s^*\bar{D}_s^*}(^3D_1)$	0.193	$0.415 + i 0.241$ (0.480)

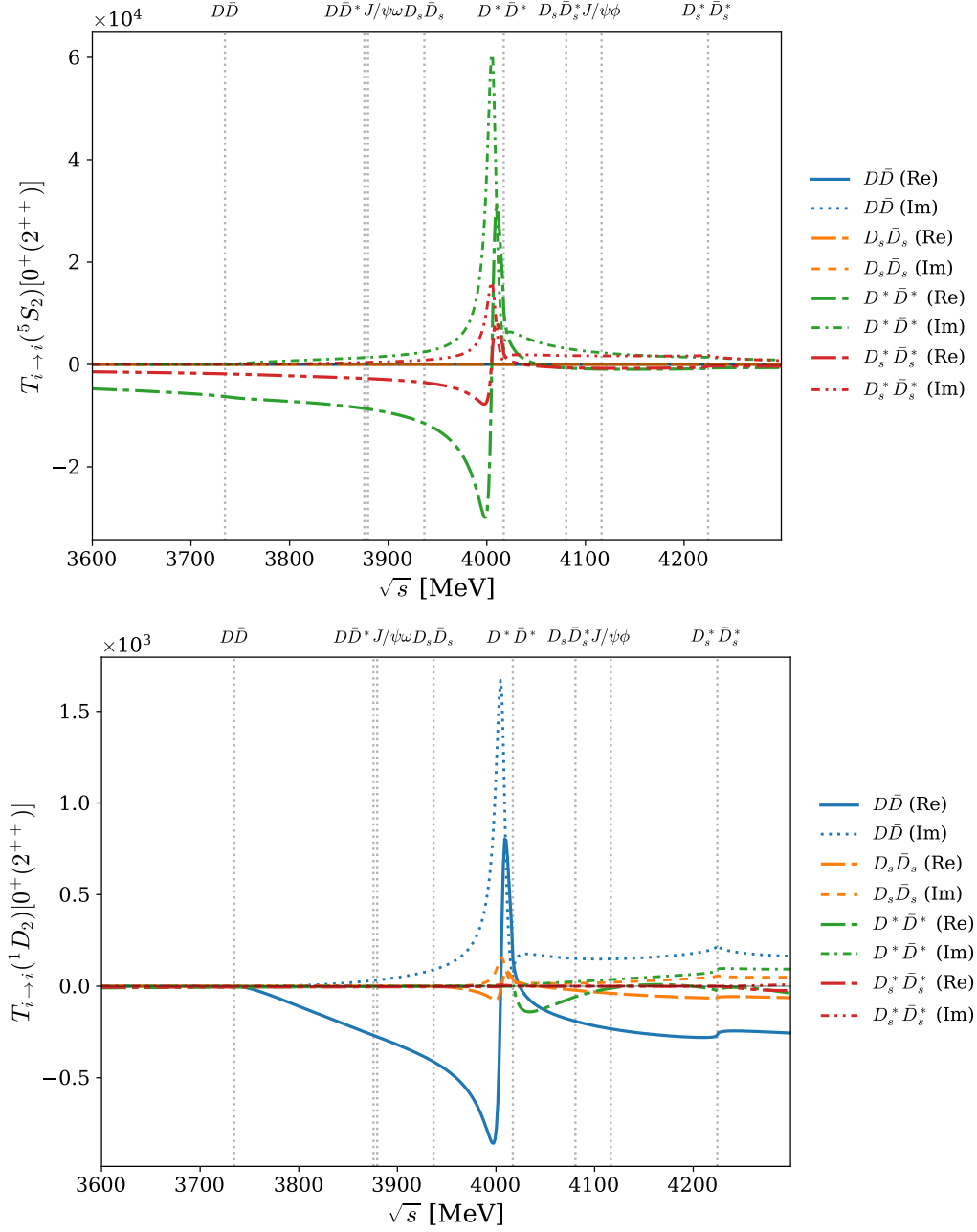


FIG. 6. Tensor transition amplitudes for diagonal elements as functions of  $\sqrt{s}$  for  $I^G(J^{PC}) = 0^+(2^{++})$  channel.

### 3. $\chi_{c2}$ $J^{PC} = 2^{++}$

Figure 6 shows the transition amplitudes for  $\chi_{c2}$  states near open-charm thresholds in the  $2^{++}$  channel. We find a narrow pole at  $\sqrt{s_R} = (4005.26 - i5.95)$  MeV, which is located between the  $D_s\bar{D}_s$  and  $D^*\bar{D}^*$  thresholds. This pole appears in both  ${}^5S_2$  and  ${}^1D_2$  partial waves, and the small imaginary part indicates a narrow width of about 12 MeV, suggesting only moderate coupled-channel effects. The residues in Table V clarify the structure of this state. The largest coupling is to  $D^*\bar{D}^*$  in  $S$  wave with  $|g_{D^*\bar{D}^*}| \simeq 1.49$ , and this pole also appears in the  $D^*\bar{D}^*$  single-channel solution. As in the  $\chi_{c0}$  and  $\chi_{c1}$  cases, the  $S$ -wave contribution from  $D_s^*\bar{D}_s^*$  is comparable to the dominant one, with  $|g_{D_s^*\bar{D}_s^*}| \simeq 0.88$ . The hidden-charm channel couplings are negligibly small. Among the  $D$ -wave contributions, the  $DD({}^1D_2)$  component is the largest with  $|g_{D\bar{D}}| \simeq 0.28$ , consistent with the peak structure seen in the lower panel of Fig. 6. We note that the pole mass lies about 70 MeV above the typical values quoted for  $\chi_{c2}(3930)$ . Whether this

state corresponds to a new tensor charmonium not yet observed experimentally remains to be seen.

TABLE V. Coupling strengths  $g_i$  for the  ${}^5S_2$  and  ${}^1D_2$  channels (in GeV). For the lower pole, imaginary parts are omitted when negligible. Unphysical or zero-coupling states are omitted for brevity.

	$g_i$	$ g_i $
$g_{J/\psi\omega}({}^5S_2)$	$0.003 - i 0.002$	0.004
$g_{D^*\bar{D}^*}({}^5S_2)$	$1.692 - i 0.216$	1.706
$g_{J/\psi\phi}({}^5S_2)$	$0.003 + i 0.000$	0.003
$g_{D_s^*\bar{D}_s^*}({}^5S_2)$	$0.877 - i 0.066$	0.879
$g_{D\bar{D}}({}^1D_2)$	$0.283 - i 0.015$	0.283
$g_{D_s\bar{D}_s}({}^1D_2)$	$0.086 - i 0.018$	0.088
$g_{D^*\bar{D}^*}({}^1D_2)$	$0.002 + i 0.001$	0.002
$g_{D_s^*\bar{D}_s^*}({}^1D_2)$	$0.019 - i 0.001$	0.019

### B. $\psi$ states: $I^G(J^{PC}) = 0^-(J^{--})$

Using the same coupled-channel framework, we analyze the transition amplitudes for the vector charmonium  $\psi$  states with several values of  $J$ . Within the energy range of interest, we do not find dynamically generated states for  $J = 0$ ,  $J = 1$ , or  $J = 2$ . Based on quark models, the well-known states in these sectors, such as  $\psi(4040)$  with  $J^{PC} = 1^{--}$ , can be regarded as having a dominant  $c\bar{c}$  core, suggesting that their description would require the inclusion of  $s$ -channel pole diagrams, which have been intentionally excluded in the present framework. As the current approach is designed to capture solely the states generated by coupled-channel dynamics, the description of these sectors could be improved by incorporating  $s$ -channel contributions, which we leave for future work. In contrast, for  $J = 3$  we find a pole above the  $D^*\bar{D}^*$  threshold in the  $J^{PC} = 3^{--}$  sector, which is less likely to be dominated by a  $c\bar{c}$  core and is therefore a more natural candidate for a dynamically generated state. We discuss this state in detail below.

#### 1. $\psi_3$ $J^{PC} = 3^{--}$

For the  $\psi_3$  state with  $J^{PC} = 3^{--}$ , the selection rules require odd orbital angular momentum  $L$  and, for identical meson pairs, even total spin  $S$ . Consequently, the allowed partial waves are restricted to  ${}^1F_3$  for  $D\bar{D}$  and  $D_s\bar{D}_s$ , and  ${}^1F_3$ ,  ${}^5P_3$ , and  ${}^5F_3$  for  $D^*\bar{D}^*$  and  $D_s^*\bar{D}_s^*$ . Non-identical pairs and hidden-charm channels couple through the  ${}^3F_3$  state. Figure 7 shows the diagonal transition amplitudes near open-charm thresholds over 3.6–4.3 GeV for  $J^{PC} = 3^{--}$  in the dominant  ${}^5P_3$  and  ${}^1F_3$  partial waves. In the  $P$ -wave transition amplitude shown in the top panel of Fig. 7, we find a rapid threshold enhancement of the elastic  $D^*\bar{D}^*$  scattering just above the  $D^*\bar{D}^*$  threshold. The elastic  $D\bar{D}$  transition amplitude in  $F$  wave also exhibits a clear peak structure just above the  $D^*\bar{D}^*$  threshold. Scanning the complex energy plane of the transition matrix, we locate a pole at  $\sqrt{s_R} = (4030.48 - i 33.33)$  MeV.

The channel coupling strengths listed in Table VI confirm the dynamical picture suggested by the line shapes. The dominant coupling is to the  $D^*\bar{D}^*({}^5P_3)$  channel with  $|g_{D^*\bar{D}^*}| \simeq 7.663$ , consistent with the pronounced threshold enhancement seen in the top panel of Fig. 7. The  $D\bar{D}({}^1F_3)$  coupling is also sizable with  $|g_{D\bar{D}}| \simeq 2.057$ , in accordance with the peak structure in the lower panel. The remaining partial-wave contributions are considerably smaller. This pole lies in the vicinity of the experimentally known  $\psi_3(3842)$  with  $J^{PC} = 3^{--}$  [29], though its mass is about 190 MeV higher, and we therefore regard it as a candidate for a new  $3^{--}$  charmonium state.

## IV. SUMMARY AND CONCLUSIONS

In the present work, we have investigated the dynamical generation of charmonium-like states with isospin  $I = 0$  and spin-parity  $J^{PC} = 0^{++}$ ,  $1^{++}$ ,  $2^{++}$ , and  $3^{--}$  in the mass range of 3.6 to 4.3 GeV, employing an off-shell coupled-channel formalism based on the Blankenbecler-Sugar reduction of the Bethe-Salpeter equation. The kernel amplitudes

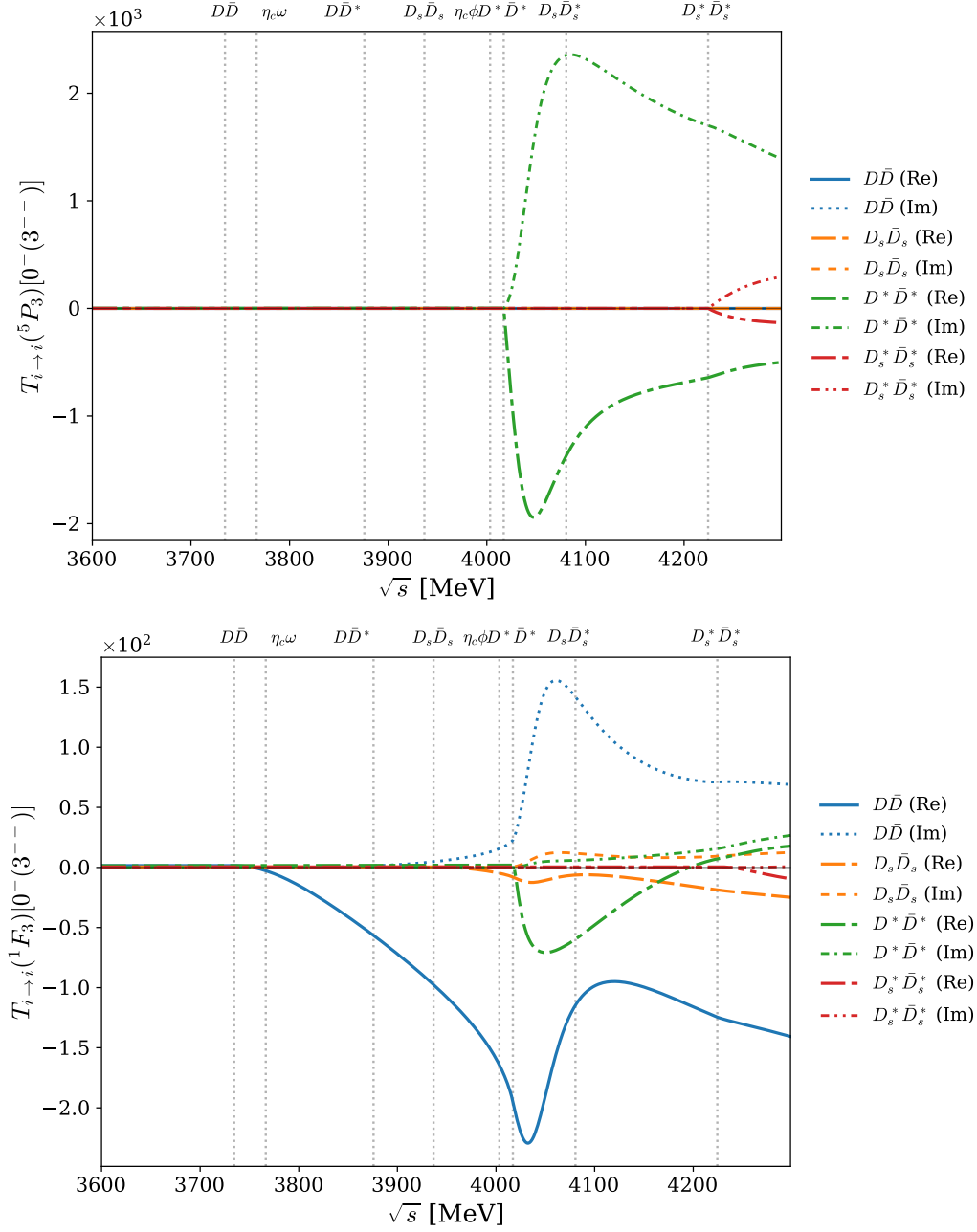


FIG. 7. Transition amplitudes for diagonal elements as functions of  $\sqrt{s}$  for  $I^G(J^{PC}) = 0^-(3^{--})$  channel in  ${}^5P_3$  and  ${}^1F_3$  partial waves.

were constructed from effective Lagrangians respecting heavy-quark spin-flavor and chiral symmetries, including  $t$ - and  $u$ -channel meson exchanges while intentionally excluding  $s$ -channel pole diagrams, so that all identified poles are generated solely by coupled-channel dynamics. Having solved the coupled-channel integral equations and scanned the transition amplitudes in the complex energy plane, we have identified six poles in total. Their properties are summarized as follows:

- In the scalar ( $0^{++}$ ) sector, two poles are identified. The first is a bound state at  $\sqrt{s_R} = 3720.5$  MeV, lying 14 MeV below the  $D\bar{D}$  threshold and generated primarily by elastic  $D\bar{D}$  scattering; no experimental evidence has been established for this state. The second pole at  $\sqrt{s_R} = (3861.34 - i22.76)$  MeV is dynamically generated by the  $D^*\bar{D}^*$  channel despite being positioned near the  $J/\psi\omega$  threshold; it is consistent in mass with  $\chi_{c0}(3860)$  and in width with  $\chi_{c0}(3915)$ , and the assignment to either candidate remains unclear.

TABLE VI. Non-zero coupling strengths  $g_i$  for the allowed partial waves of the  $\psi_3$  state (in GeV). Unphysical partial waves forbidden by spin, parity, and C-parity conservation are omitted.

	$g_i$	$ g_i $
$g_{D^*\bar{D}^*({}^5P_3)}$	$2.883 - i 7.100$	7.663
$g_{D_s^*\bar{D}_s^*({}^5P_3)}$	$0.004 - i 0.002$	0.004
$g_{D\bar{D}({}^1F_3)}$	$1.326 - i 1.573$	2.057
$g_{D_s\bar{D}_s({}^1F_3)}$	$0.351 - i 0.486$	0.599
$g_{D^*\bar{D}^*({}^1F_3)}$	$0.289 - i 0.222$	0.364
$g_{D_s^*\bar{D}_s^*({}^1F_3)}$	$2.661 \times 10^{-4} - i 0.001$	$1.228 \times 10^{-3}$
$g_{D\bar{D}^*({}^3F_3)}$	$0.008 + i 9.985 \times 10^{-5}$	0.008
$g_{\eta_c\omega({}^3F_3)}$	$1.874 \times 10^{-4} - i 8.331 \times 10^{-5}$	$2.051 \times 10^{-4}$
$g_{D_s\bar{D}_s^*({}^3F_3)}$	$2.152 \times 10^{-6} + i 5.338 \times 10^{-4}$	$5.338 \times 10^{-4}$
$g_{\eta_c\phi({}^3F_3)}$	0	0
$g_{D^*\bar{D}^*({}^5F_3)}$	$0.702 - i 0.245$	0.744
$g_{D_s^*\bar{D}_s^*({}^5F_3)}$	$8.869 \times 10^{-4} - i 0.002$	0.002

- In the axial-vector ( $1^{++}$ ) sector, we reproduce a narrow bound state at  $\sqrt{s_R} = 3874.26$  MeV, lying almost exactly at the  $D\bar{D}^*$  threshold and generated predominantly by elastic  $D\bar{D}^*$  scattering. This state is a natural candidate for the well-known  $\chi_{c1}(3872)$ . The coupling analysis reveals a nontrivial channel structure beyond a pure  $D\bar{D}^*$  molecular picture, with sizable contributions from  $D^*\bar{D}^*$  and  $D_s\bar{D}_s^*$ . A second, broader pole is found at  $\sqrt{s_R} = (3961.40 - i 32.25)$  MeV, dominated by the  $D^*\bar{D}^*({}^3S_1)$  channel, and is identified as a plausible candidate for the  $X(3940)$ .
- In the tensor ( $2^{++}$ ) sector, we find a narrow pole at  $\sqrt{s_R} = (4005.26 - i 5.95)$  MeV, lying below the  $D^*\bar{D}^*$  threshold and appearing in both  ${}^5S_2$  and  ${}^1D_2$  partial waves. The dominant coupling is to  $D^*\bar{D}^*$  in  $S$  wave, and the pole also appears in the  $D^*\bar{D}^*$  single-channel, indicating that coupled-channel effects are moderate. The pole mass lies about 70 MeV above the typical values quoted for  $\chi_{c2}(3930)$ . This state has not yet been observed experimentally.
- In the vector ( $3^{--}$ ) sector, we find a pole at  $\sqrt{s_R} = (4030.48 - i 33.33)$  MeV, above the  $D^*\bar{D}^*$  threshold. This state is dominantly coupled to  $D^*\bar{D}^*$  in the  ${}^5P_3$  partial wave, with a sizable  $D\bar{D}({}^1F_3)$  contribution. We regard this as a candidate for a new  $3^{--}$  charmonium state, distinct from  $\psi_3(3842)$ , whose mass lies about 190 MeV lower.

A common pattern emerging from the present analysis is the crucial role of the  $D^*\bar{D}^*$  channel in driving the dynamical generation of the resonances across all spin-parity sectors investigated. In particular, the  $D_s^*\bar{D}_s^*$  channel consistently provides a subleading but nonnegligible contribution, reflecting the importance of hidden-strangeness components in the coupled-channel dynamics. We note that no dynamically generated poles are found in the  $\psi$  sectors with  $J = 0, 1$ , and 2. This may be related to the fact that the well-known states in these sectors, such as  $\psi(4040)$ , are widely regarded as having a dominant  $c\bar{c}$  core, whose description would require the inclusion of  $s$ -channel contributions not considered in the present framework. A more complete treatment incorporating both  $s$ -channel pole diagrams and coupled-channel dynamics would be needed to describe the full charmonium spectrum, and we leave this for future work.

## ACKNOWLEDGMENTS

The present work was supported by the National Research Foundation of Korea (NRF) grant funded by the Korea government under Grant No. RS-2025-02634319 (HJK) and RS-2025-00513982 (HChK).

---

[1] S. K. Choi *et al.* (Belle), Phys. Rev. Lett. **91**, 262001 (2003), arXiv:hep-ex/0309032.

- [2] R. F. Lebed, R. E. Mitchell, and E. S. Swanson, *Prog. Part. Nucl. Phys.* **93**, 143 (2017), arXiv:1610.04528 [hep-ph].
- [3] F.-K. Guo, C. Hanhart, U.-G. Meißner, Q. Wang, Q. Zhao, and B.-S. Zou, *Rev. Mod. Phys.* **90**, 015004 (2018), [Erratum: *Rev. Mod. Phys.* **94**, 029901 (2022)], arXiv:1705.00141 [hep-ph].
- [4] F.-K. Guo, X.-H. Liu, and S. Sakai, *Prog. Part. Nucl. Phys.* **112**, 103757 (2020), arXiv:1912.07030 [hep-ph].
- [5] Y. Yamaguchi, A. Hosaka, S. Takeuchi, and M. Takizawa, *J. Phys. G* **47**, 053001 (2020), arXiv:1908.08790 [hep-ph].
- [6] H.-X. Chen, W. Chen, X. Liu, Y.-R. Liu, and S.-L. Zhu, *Rept. Prog. Phys.* **86**, 026201 (2023), arXiv:2204.02649 [hep-ph].
- [7] L. Meng, B. Wang, G.-J. Wang, and S.-L. Zhu, *Phys. Rept.* **1019**, 1 (2023), arXiv:2204.08716 [hep-ph].
- [8] E. Eichten, K. Gottfried, T. Kinoshita, K. D. Lane, and T.-M. Yan, *Phys. Rev. D* **17**, 3090 (1978), [Erratum: *Phys. Rev. D* **21**, 313 (1980)].
- [9] T. Barnes, S. Godfrey, and E. S. Swanson, *Phys. Rev. D* **72**, 054026 (2005), arXiv:hep-ph/0505002.
- [10] B.-Q. Li and K.-T. Chao, *Phys. Rev. D* **79**, 094004 (2009), arXiv:0903.5506 [hep-ph].
- [11] B. Wang, H. Xu, X. Liu, D.-Y. Chen, S. Coito, and E. Eichten, *Front. Phys. (Beijing)* **11**, 111402 (2016), arXiv:1507.07985 [hep-ph].
- [12] L. Cao, Y.-C. Yang, and H. Chen, *Few Body Syst.* **53**, 327 (2012), arXiv:1206.3008 [hep-ph].
- [13] T. Wang, G.-L. Wang, H.-F. Fu, and W.-L. Ju, *JHEP* **07**, 120 (2013), arXiv:1305.1067 [hep-ph].
- [14] J.-B. Cheng, S.-Y. Li, Y.-R. Liu, Z.-G. Si, and T. Yao, *Chin. Phys. C* **45**, 043102 (2021), arXiv:2008.00737 [hep-ph].
- [15] M. Praszalowicz, *Phys. Rev. D* **106**, 114005 (2022), arXiv:2208.08602 [hep-ph].
- [16] J. Zhang, J.-B. Wang, G. Li, C.-S. An, C.-R. Deng, and J.-J. Xie, *Eur. Phys. J. C* **82**, 1126 (2022), arXiv:2209.13856 [hep-ph].
- [17] M. Kucab and M. Praszalowicz, *Phys. Rev. D* **109**, 076005 (2024), arXiv:2402.04169 [hep-ph].
- [18] M. N. Anwar and T. J. Burns, *Phys. Lett. B* **847**, 138248 (2023), arXiv:2309.03309 [hep-ph].
- [19] Q. Meng, E. Hiyama, M. Oka, A. Hosaka, and C. Xu, *Phys. Lett. B* **846**, 138221 (2023), arXiv:2308.05466 [nucl-th].
- [20] W.-C. Dong and Z.-G. Wang, *Nucl. Phys. B* **1012**, 116828 (2025), arXiv:2407.19383 [hep-ph].
- [21] S. Clymton and H.-C. Kim, *Phys. Rev. D* **106**, 114015 (2022), arXiv:2208.04124 [hep-ph].
- [22] S. Clymton and H.-C. Kim, *Phys. Rev. D* **108**, 074021 (2023), arXiv:2305.14812 [hep-ph].
- [23] S. Clymton and H.-C. Kim, *Phys. Rev. D* **110**, 114002 (2024), arXiv:2409.02420 [hep-ph].
- [24] S. Clymton, H.-C. Kim, and T. Mart, *Phys. Rev. D* **110**, 094014 (2024), arXiv:2408.04166 [hep-ph].
- [25] S. Clymton, H.-C. Kim, and T. Mart, *Phys. Rev. D* **112**, 094024 (2025), arXiv:2508.12293 [hep-ph].
- [26] S. Clymton, H.-C. Kim, and T. Mart, *Phys. Rev. D* **112**, 034015 (2025), arXiv:2506.23587 [hep-ph].
- [27] H.-J. Kim and H.-C. Kim, *PTEP* **2024**, 073D01 (2024), arXiv:2310.13370 [hep-ph].
- [28] H.-J. Kim and H.-C. Kim, *Phys. Rev. D* **112**, 094025 (2025), arXiv:2507.09191 [hep-ph].
- [29] S. Navas *et al.* (Particle Data Group), *Phys. Rev. D* **110**, 030001 (2024).
- [30] R. Blankenbecler and R. Sugar, *Phys. Rev.* **142**, 1051 (1966).
- [31] R. Aaron, R. D. Amado, and J. E. Young, *Phys. Rev.* **174**, 2022 (1968).
- [32] M. B. Wise, *Phys. Rev. D* **45**, R2188 (1992).
- [33] T.-M. Yan, H.-Y. Cheng, C.-Y. Cheung, G.-L. Lin, Y. C. Lin, and H.-L. Yu, *Phys. Rev. D* **46**, 1148 (1992), [Erratum: *Phys. Rev. D* **55**, 5851 (1997)].
- [34] R. Casalbuoni, A. Deandrea, N. Di Bartolomeo, R. Gatto, F. Feruglio, and G. Nardulli, *Phys. Rept.* **281**, 145 (1997), arXiv:hep-ph/9605342.
- [35] M. Bando, T. Kugo, and K. Yamawaki, *Nucl. Phys. B* **259**, 493 (1985).
- [36] S. Ahmed *et al.* (CLEO), *Phys. Rev. Lett.* **87**, 251801 (2001), arXiv:hep-ex/0108013.
- [37] C. Isola, M. Ladisa, G. Nardulli, and P. Santorelli, *Phys. Rev. D* **68**, 114001 (2003), arXiv:hep-ph/0307367.
- [38] H.-J. Kim and H.-C. Kim, *Phys. Rev. D* **102**, 014026 (2020), arXiv:1912.11622 [hep-ph].
- [39] K. Kawarabayashi and M. Suzuki, *Phys. Rev. Lett.* **16**, 255 (1966).
- [40] Riazuddin and Fayyazuddin, *Phys. Rev.* **147**, 1071 (1966).
- [41] H.-C. Kim, J. W. Durso, and K. Holinde, *Phys. Rev. C* **49**, 2355 (1994).
- [42] J.-Y. Kim and H.-C. Kim, *Phys. Rev. D* **97**, 114009 (2018), arXiv:1803.04069 [hep-ph].
- [43] J.-Y. Kim, H.-C. Kim, G.-S. Yang, and M. Oka, *Phys. Rev. D* **103**, 074025 (2021), arXiv:2101.10653 [hep-ph].
- [44] H.-Y. Cheng, C.-K. Chua, and A. Soni, *Phys. Rev. D* **71**, 014030 (2005), arXiv:hep-ph/0409317.
- [45] S. Clymton, H.-C. Kim, and T. Mart, *Phys. Rev. D* **112**, 014041 (2025), arXiv:2504.07693 [hep-ph].